BBA - Bioenergetics 1859 (2018) 57–68

Contents lists available at ScienceDirect

BBA - Bioenergetics

journal homepage: www.elsevier.com/locate/bbabio

Spectrally decomposed dark-to-light transitions in a PSI-deficient mutant of *Synechocystis* sp. PCC 6803

Alonso M. Acuña[a,1], Pascal van Alphen[b,1], Filipe Branco dos Santos[b], Rienk van Grondelle[a], Klaas J. Hellingwerf[b], Ivo H.M. van Stokkum[a,*]

[a] Institute for Lasers, Life and Biophotonics, Faculty of Sciences, Vrije Universiteit Amsterdam, De Boelelaan 1081, 1081 HV, Amsterdam, The Netherlands.
[b] Swammerdam Institute for Life Sciences, University of Amsterdam, 1098 XH, Amsterdam, The Netherlands.

ARTICLE INFO

Keywords:
Cyanobacteria
Spectrally-resolved fluorometry
Singular Value Decomposition
Time-resolved spectroscopy

ABSTRACT

Cyanobacterial thylakoid membranes are known to host photosynthetic and respiratory complexes. This hampers a straight forward interpretation of the highly dynamic fluorescence originating from photosynthetic units. The present study focuses on dark-to-light transitions in whole cells of a PSI-deficient mutant of the cyanobacterium *Synechocystis* sp. PCC 6803. The time-dependent cellular fluorescence spectrum has been measured, while having previously exposed the cells to different conditions that affect respiratory activity. The analysis method used allows the detected signal to be decomposed in a few components that are then assigned to functional emitting species. Additionally, we have worked out a minimal mathematical model consisting of sensible postulated species to interpret the recorded data. We conclude that the following two functional complexes play a major role: a phycobilisome antenna complex coupled to a PSII dimer with either two or no closed reaction centers. Crucially, we present evidence for an additional species capable of strongly quenching fluorescence, whose formation requires the presence of oxygen.

1. Introduction

The cyanobacterial thylakoid membrane harbors both photosynthetic and respiratory units, making electron transport a highly dynamic and complex process [1–3]. In the cyanobacterium *Synechocystis* sp. PCC 6803 (hereafter *Synechocystis*), three interwoven electron transport routes are typically regarded as dominant: *i*) linear photosynthetic electron transport involving the photosystems (PS) I and II, the cytochrome b_6f complex (hereafter cyt b_6f), the plastoquinone (PQ) and plastocyanin (PC) pools, *ii*) respiratory transport mainly involving the electron donors succinate dehydrogenase (SDH) and the type-I NAD(P)H dehydrogenase (NDH-1), cytochrome *c*, the cytochrome *bd*-type quinol oxidase (Cyd) and the *aa3*-type cytochrome *c* oxidase (COX) and *iii*) cyclic electron transport around PSI [4–7]. Additional possibilities include alternate respiratory terminal oxidases (ARTO) and electron transfer from PSI to flavodiiron proteins Flv1 and Flv3 as well as NDH-1 [8–13]. A balanced interplay of all these units is necessary in order to, for example, generate a favorable ATP:NADPH flux-ratio, typically of 3:2 [14], or alter this ratio to accommodate photoprotective and/or repair responses under stress conditions. Photoprotective mechanisms in *Synechocystis* reportedly include non-photochemical fluorescence quenching (NPQ) via the orange carotenoid protein (OCP) and *state transitions* (ST) [3,15]. While the former is a response to (high) blue light intensity that leads to photoactivation of OCP, which in turn, binds to the phycobilisome (PB) thereby quenching it [16–18], the latter refers to a change in the rate of excitation energy transfer (EET) to PSII vis-à-vis PSI [19–21]. In other words, while OCP activity enables an additional EET channel to avoid excitation energy reaching the reaction centers (RCs) in the first place, STs are a subtly regulated response to re-balance the EET ratio between the two photosystems during, for instance, a sudden change in the intensity of the incident radiation. Thus, PSI both plays a pivotal role in EET regulation and is a crucial vehicle for electron transport across the thylakoid membrane.

Cells of a PSI-deficient mutant of *Synechocystis* were subject to investigation in a recent study focusing on changes in chlorophyll (Chl) *a* fluorescence as a result of dark-to-light transitions [22]. Therein, the authors reported a quenched species, appearing under illumination conditions that ensured that OCP could not have been activated. This result unavoidably revives the fundamental question asked many years ago already by Vermaas et al. [23]: what happens to the excitations in the absence of PSI when the PSIIRC is closed? Since both OCP-related fluorescence quenching and ST must be ruled out, Acuña et al. [22]

* Corresponding author.
E-mail address: ivo@few.vu.nl (I.H.M. van Stokkum).
[1] Authors have contributed equally to this work.

https://doi.org/10.1016/j.bbabio.2017.11.002
Received 9 July 2017; Received in revised form 23 October 2017; Accepted 9 November 2017
Available online 11 November 2017
0005-2728/

postulated a third quenching mechanism in order to explain the overall fluorescence decrease: a high-light protein (Hlip) would be at its origin. Hlips have indeed been suggested to act as non-photochemical quenchers in *Synechocystis* [24] and there is conclusive evidence that HliD, one of the members of the Hlip-family, binds Chlorophyll *a* (Chl *a*) and β-carotene (β-car), thus enabling a dissipative channel with energy being directly transferred from a Chl *a* Q_y state to a β-car S_1 state [25,26]. Besides, in the specific case of the PSI-deficient mutant of *Synechocystis*: *i*) Hlip-containing cells have been shown to evolve much less singlet oxygen than the corresponding control strain [27], confirming the photoprotective role of HliD, and *ii*) the carotenoid content of HliD-containing fractions has been found to be relatively high [28], which makes the assumption of an HliD-related quenching channel all the more plausible.

The central aim of this study is to elucidate how cells of a PSI-deficient mutant of *Synechocystis* are able to cope with light stress during a dark-to-light transition. We do this by tracking the emitted cellular fluorescence spectrum over time [29,30]. The obtained results are analyzed (Section 3.1) using a method based on the Singular Value Decomposition (SVD) previously demonstrated in [22]. Then, we discuss the SVD-based results in terms of the parameters of a mathematical model (Section 3.2). The only photosynthetic fluorescent units present in the sample of this strain are the phycocyanin-containing PB antenna and the Chl *a*-containing PSII dimers. Any fluorescence dynamics should therefore be explained in terms of these species only. In the following *Gedankenexperiment* we make an attempt to anticipate which species will be manifested and how: *i*) a PB unable to transfer excitation energy to PSII should be visible as a pure PB-spectrum with a very high fluorescence quantum yield; *ii*) if the PB is coupled to a PSII-dimer while both RCs are closed, we also expect a high quantum yield, though with an additional chlorophyll-derived 680 nm signature; *iii*) in case of a functional PB-PSII complex with two photochemically (open) quenched RCs, we would expect a less strong 680 nm signature and a low fluorescence quantum yield; *iv*) should only one of the RCs in the PSII dimer be closed while the other would remain open, we would expect a fluorescence quantum yield that lies somewhere between *ii*) and *iii*); *v*) a PB-PSII complex being non-photochemically quenched would result in a low fluorescence quantum yield. Fig. 1 schematically depicts these species. We set out to measure time-resolved fluorescence spectra of whole cells of the PSI-deficient mutant of *Synechocystis* after preparing the cells with different dark-adaptation (DA) times, so as to systematically affect its respiratory activity. This resulted in the identification of a novel quencher that is insensitive to the respiratory inhibitor potassium cyanide (KCN), yet requires oxygen to function.

2. Materials and methods

2.1. Cell cultures

The PSI-deficient mutant of *Synechocystis* [31] was a gift from prof. C. Funk (Umeå University, Sweden) and was stored at − 80 °C in 15% glycerol. Prior to preparing a liquid culture, cells were streaked on agar plates containing BG-11 (Sigma) supplemented with 0.3% sodium thiosulfate, 35 μg/mL chloramphenicol and 10 mM glucose. The strain appeared incompatible with our usual agar, requiring the plates to be solidified using Difco Granulated agar (BD). The plates were incubated in an incubator (Versatile Environmental Test Chamber MLR-350H, Sanyo) with a humidified atmosphere of elevated CO_2 (2%) kept at 30 °C. Incident light intensity was reduced to below 5 μmol photons $m^{-2} s^{-1}$ by covering the plates with layers of paper.

Liquid cultures were prepared by inoculating 25 mL modified BG-11 (BG-11-PC, van Alphen et al. manuscript in preparation) supplemented with 10 mM glucose, 25 mM 1,4-Piperazinedipropanesulfonic acid (PIPPS)-KOH buffered at pH 8.0, 5 μg/mL chloramphenicol in a 100-mL flask (FB33131, Fisherbrand). The nitrogen source was $NaNO_3$ except for the batch of cells discussed in Section 3.2.2 where NH_4Cl was used instead. The flasks were covered in multiple layers of paper to reduce the incident light intensity to below 5 μmol photons $m^{-2} s^{-1}$ and were placed in a shaking incubator (Innova 43, New Brunswick Scientific), equipped with a custom LED panel containing LEDs of 632 nm (orange-red) and 451 nm (blue, both 8 nm full width at half maximum) at 120 rpm and 30 °C.

2.2. Spectrally resolved fluorescence induction

The multiple LED set-up described in [22,32] was placed right near the facilities where the *Synechocystis* cells were grown, ensuring thereby that the cells were in proper physiological conditions during the experiments. The illumination protocols (Fig. S 1) have been applied to ΔPSI cells of *Synechocystis*, taken from the same batch, diluted to an optical density at 730 nm (OD_{730}) of 0.4 in fresh medium (the only exception being Fig. 12). Two background (590 nm) light intensities

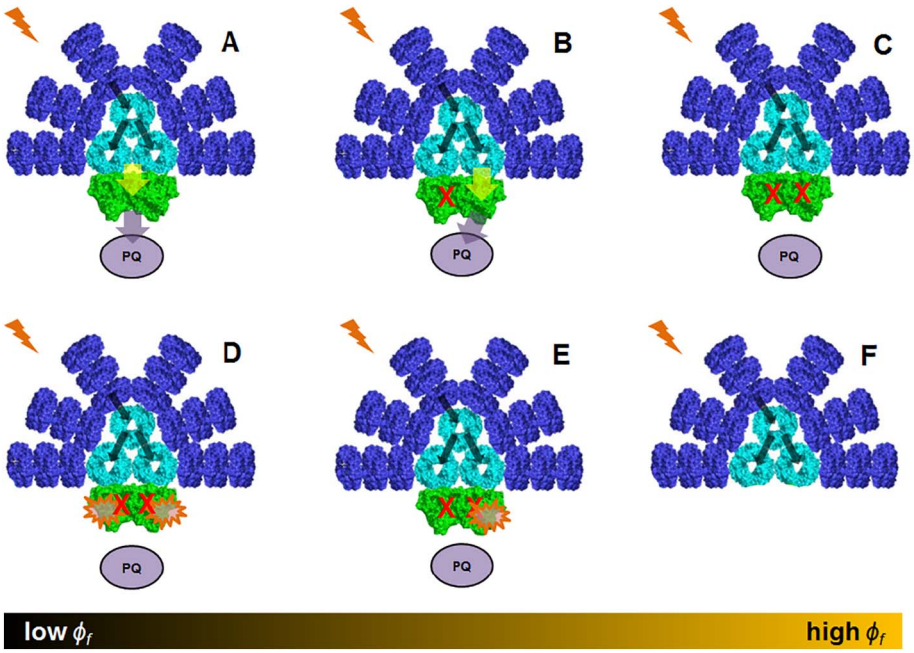

Fig. 1. Visualization of possible fluorescent species in the *Synechocystis* ΔPSI mutant and their expected fluorescence quantum yield ϕ_f. Black arrows represent intra-PB EET; yellow arrows represent EET from the PB core to PSII; purple arrows represent electron transfer to the PQ pool. An "X" stands for a closed RC. Low ϕ_f values are expected from PB-PSII complexes quenched either photochemically (A) with both RCs transferring electrons to the PQ pool (open) or non-photochemically by an Hlip-type quencher (D) bound to PSII with its RCs closed. High ϕ_f values are expected from PB-PSII complexes with both RCs closed and unquenched (C) or functionally uncoupled PB (F). In case one of the RCs of the PSII dimer is closed and unquenched while the other is open (B) or quenched (E), we expect an intermediate ϕ_f value.
(Adapted from Liu [1]).

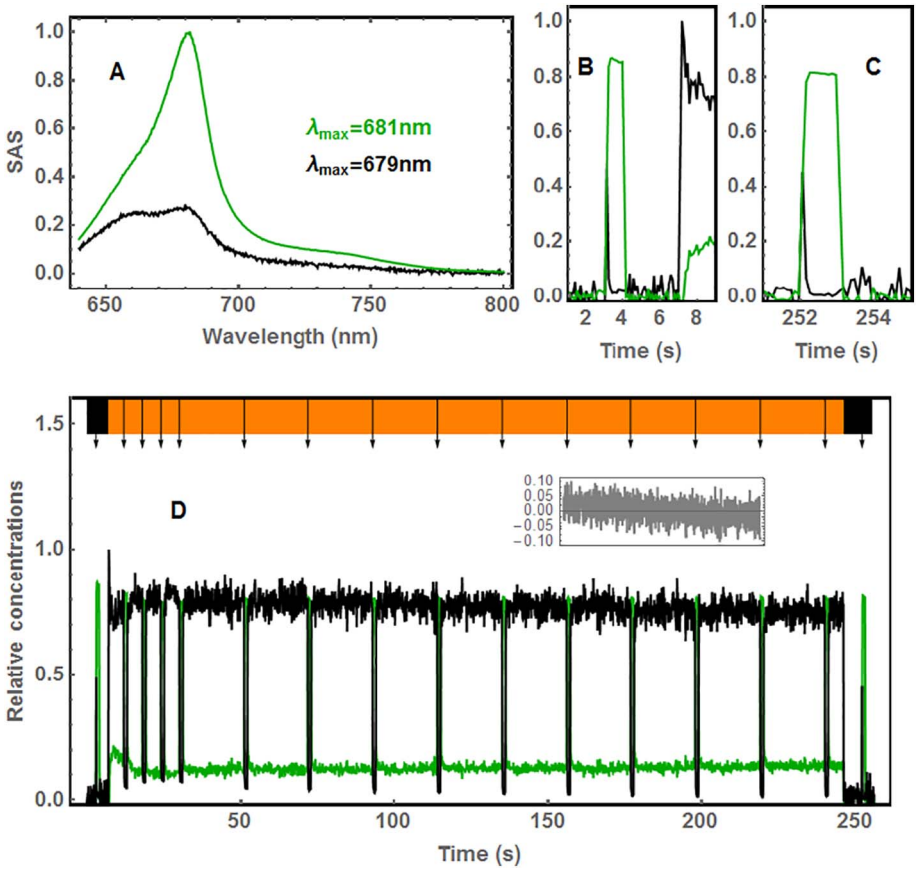

Fig. 2. Spectral decomposition of fluorescence spectra of 34 min dark-adapted ΔPSI cells exposed to low light background illumination and ambient O_2. (A) The SAS obtained after transformation of the singular vectors (shown in Fig. S 2). Panels B and C show a zoom view of the first 9 s and of the last pulse, respectively. (D) Time profiles. *Key*: *orange*: 50 μmol photons $m^{-2} s^{-1}$; *black*: darkness. The colored bar on top illustrates the light regime with arrows indicating the beginning of a saturation pulse. *Inset*: The average deviation in the sum of concentrations from unity.

Table 1
Average (of seven points) levels of c_1 and c_2 at three different spots of the light protocol: first and last saturation pulses as well as average F_s level just before the background is turned off.

DA (min) [Figure]	First pulse		Final F_S		Last pulse	
	c_1	c_2	c_1	c_2	c_1	c_2
50 μmol photons $m^{-2} s^{-1}$						
34 [2]	0.02	0.86	0.84	0.16	0.03	0.81
5 [S 4]	0.03	0.97	0.84	0.16	0.07	0.93
1 [S 4]	0.07	0.93	0.84	0.16	0.04	0.89
450 μmol photons $m^{-2} s^{-1}$						
34(+ KCN) [3]	0.02	0.98	0.28	0.72	0.28	0.72
34(+ N_2/CO_2) [5]	0.03	0.97	0.29	0.71	0.03	0.93
1(+ N_2/CO_2) [S 8]	0.01	0.99	0.34	0.55	0	0.84
34 [6D]	0.02	0.98	0.60	0.40	0.32	0.68
5 [6D]	0.02	0.98	0.56	0.44	0.31	0.69
1 [6D]	0.02	0.98	0.40	0.60	0.18	0.82

were used: 50 μmol photons $m^{-2} s^{-1}$ (referred to as *low* light; see Fig. S 1A) and 450 μmol photons $m^{-2} s^{-1}$ (referred to as *high* light; see Fig. S 1B). The light intensity during the saturating pulses was 1300 μmol photons $m^{-2} s^{-1}$. Each pulse (1 s) consists of ten data points since the time resolution is 100 ms. Cells have undergone varying DA times prior to application of the illumination protocol. Also, we have measured under conditions preventing respiratory electron transfer to oxygen, realized in two different ways: chemically, using KCN (1 mM final concentration) which is known to inhibit respiratory activity [33,34]; and physically, by bubbling an N_2/CO_2 mixture into the cuvette containing the sample to generate an O_2-deprived environment. Under these micro-oxic conditions, the oxygen concentration is assumed to be well below the K_m of the terminal oxidases, such that the terminal oxidases are effectively shut down.

2.3. Additional elements of data analysis

Here we describe an extension of the spectral decomposition methods that have been described in [22]. Acquired fluorescence spectra (p wavelengths) at m time points can be represented by an ($m \times p$) data matrix Ψ. The Singular Value Decomposition (SVD) procedure [35] decomposes Ψ according to:

$$\Psi = \boldsymbol{U} \cdot \boldsymbol{S} \cdot \boldsymbol{V}^{\mathbf{T}} \quad (1)$$

into an ($m \times m$) matrix $\boldsymbol{U}$, where the m columns are called the *left singular vectors* (*lsv*); the ($m \times p$) diagonal matrix $\boldsymbol{S}$ whose diagonal elements (s_1, s_2, s_3…) are called the singular values and the transpose of the ($p \times p$) matrix $\boldsymbol{V}$, $\boldsymbol{V}^{\mathbf{T}}$, where the p rows are called the *right singular vectors* (*rsv*). Time-dependent characteristics are contained in the *lsv*, while the *rsv* are a linear combination of the species associated spectra (SAS). The original matrix Ψ can be satisfactorily reconstructed by means of the n most significant singular vectors yielding a ($nt \times n\lambda$) matrix Ψ_n. In Acuña, Kaňa, Gwizdala, Snellenburg, van Alphen, van Oort, Kirilovsky, van Grondelle and van Stokkum [22] data matrices of rank $n = 2$ were analyzed. While the core of the method remains the same, we also present data matrices that are of rank $n = 3$, meaning that the transformation matrix applied to the singular vectors had to be correspondingly expanded.

We seek a mathematical transformation $\Psi_n = \boldsymbol{U} \cdot \boldsymbol{S} \cdot (A^{-1} \cdot A) \cdot \boldsymbol{V}^{\mathbf{T}}$ to resolve the SAS and their time-dependent concentrations. For a rank

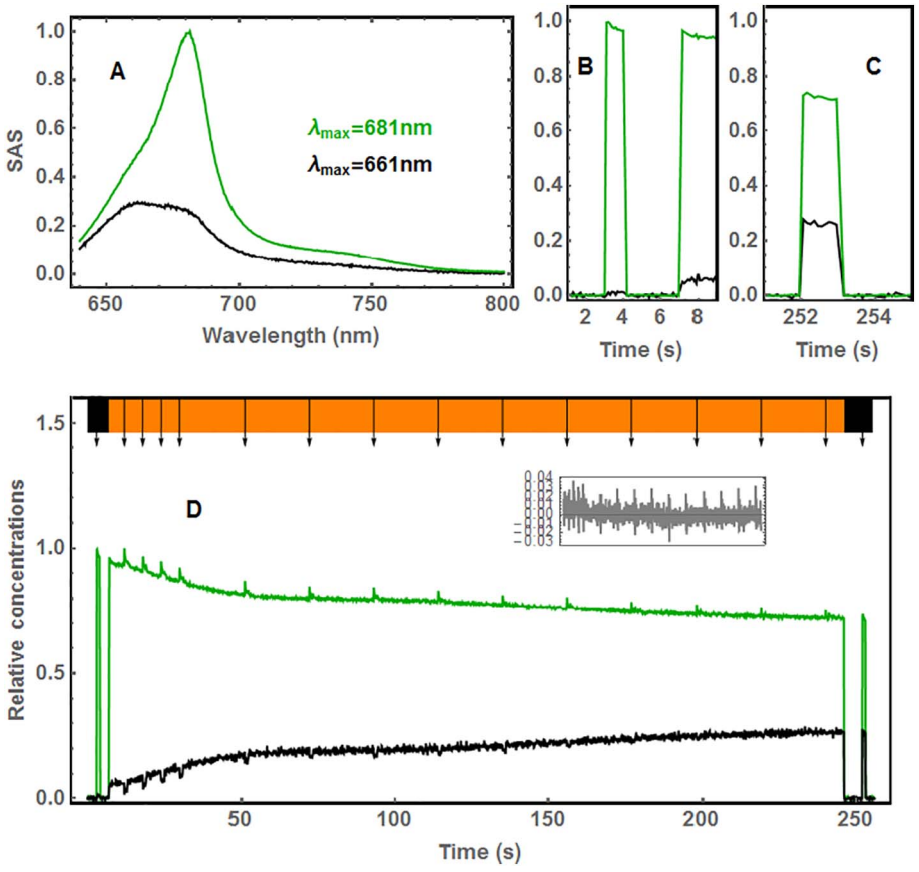

Fig. 3. Spectral decomposition of fluorescence spectra of 34 min dark-adapted ΔPSI cells exposed to high light background illumination, ambient O_2 and treated with KCN. (A) The SAS (Black: SAS_1; green: SAS_2) obtained after transformation of the singular vectors (shown in Fig. S 3). Panels B and C show a zoom view of the first and last pulse. (D) Time profiles. *Key*: *orange*: 450 μmol photons $m^{-2} s^{-1}$; *black*: darkness. The colored bar on top illustrates the light regime with arrows indicating the beginning of a saturation pulse. *Inset*: The average deviation in the sum of concentrations from unity.

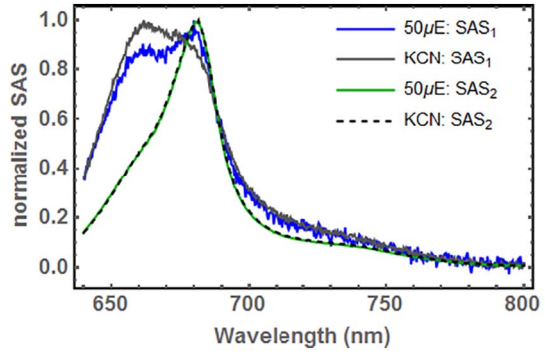

Fig. 4. Normalized SAS of the experiments shown in Figs. 2 and 3. While SAS_2 (solid green and dashed black) are virtually identical, SAS_1 from the KCN experiment (solid gray) has slightly weaker fluorescence around 680 nm than SAS_1 from cells without KCN which were exposed to 50 μmol photons $m^{-2} s^{-1}$ (solid blue).

$n = 3$ matrix, A has the form:

$$A = \begin{pmatrix} 1 & a_{12} & a_{13} \\ a_{21} & a_{22} & a_{23} \\ a_{31} & a_{32} & a_{33} \end{pmatrix} \quad (2)$$

and the final decomposition of $\Psi_{(n=3)}$ is expressed as a linear combination of three $nt \times 1$ vectors corresponding to the concentrations and the $1 \times n\lambda$ vectors corresponding to the $SAS_{n\lambda}$:

$$\Psi_{(n=3)} = c_{t1}SAS_{1\lambda} + c_{t2}SAS_{2\lambda} + c_{t3}SAS_{3\lambda} \quad (3)$$

Hereafter, we will refer to these vectors using the simplified notation: c_1, c_2, c_3, SAS_1, SAS_2 and SAS_3. Furthermore, a number of criteria are followed to judge whether these transformed vectors are biophysically meaningful. With the expansion to a rank $n = 3$ matrix, the number of parameters to be estimated increases; this is why, additionally to the criteria presented in our previous work [22], we have added, for each SAS, SAS *smoothness*–penalties:

$$\text{penalty}_{smoothness} = \sum_j w_j \cdot \left| \int \frac{\partial^2}{\partial \lambda^2} SAS_j(\lambda) \right| \quad (4)$$

This is one among other contributions to the objective function that we seek to minimize. See the SI for the explicit objective function used in this work. For a rank $n = 2$ matrix, which is applicable for most of the data sets presented here, the description is simpler, and A has the form:

$$A = \begin{pmatrix} 1 & a_{12} \\ a_{21} & a_{21} \cdot a_{22} \end{pmatrix} \quad (5)$$

and the final decomposition of $\Psi_{(n=2)}$ is expressed as:

$$\Psi_{(n=2)} = c_{t1}SAS_{1\lambda} + c_{t2}SAS_{2\lambda} \quad (6)$$

Finally, each concentration value c_{nt} output at the position t that corresponds to a saturation pulse is multiplied by a parameter p_f that accounts for the difference in light intensity between the background illumination and the saturation pulse. Thus, relative concentrations that are independent of the light intensity are estimated.

3. Results and discussion

3.1. Results from SVD analysis

In this section, we discuss results obtained following different protocols. First, we show results of ΔPSI cells exposed to ambient oxygen and 50 μmol photons $m^{-2} s^{-1}$ of 590 nm that we refer to as low-light experiments. Then, we show results from samples exposed to 450 μmol photons $m^{-2} s^{-1}$ (high light). The cells were either treated with KCN to inhibit the terminal oxidases or exposed to a mixture of N_2/CO_2 to generate an O_2-deprived environment in which the terminal

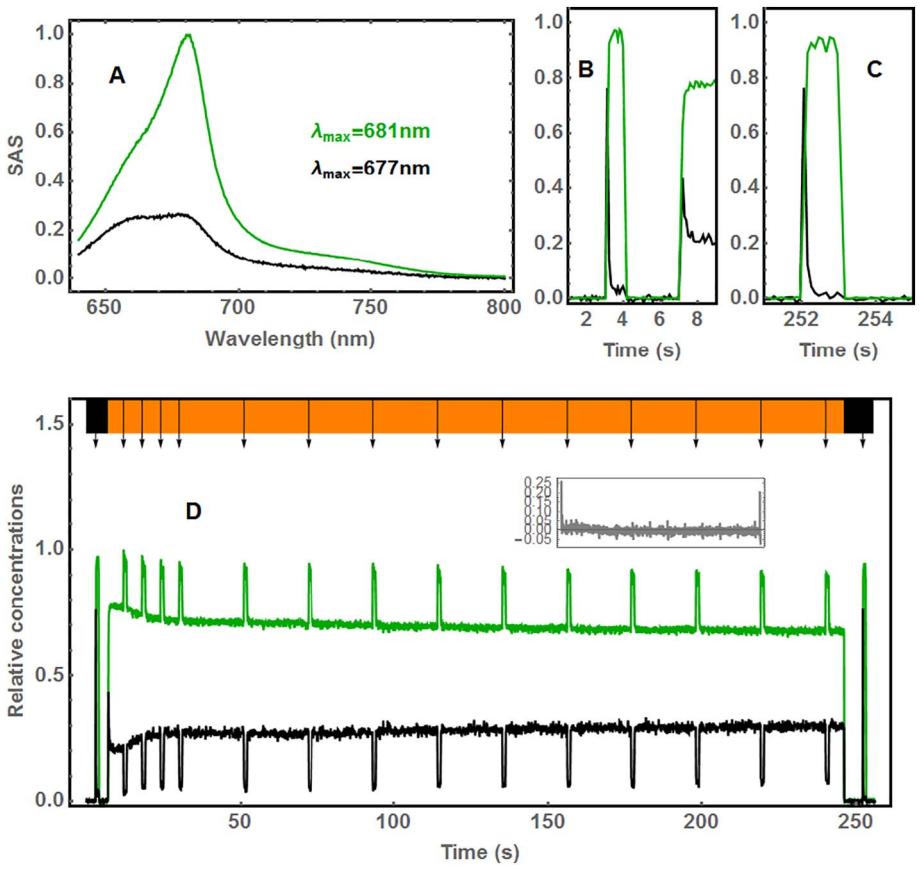

Fig. 5. Spectral decomposition of fluorescence spectra of 34 min dark-adapted ΔPSI cells exposed to high light background illumination under microoxic conditions. (A) The SAS (Black: SAS_1; green: SAS_2) obtained after transformation of the singular vectors (shown in Fig. S 5). Panels B and C show a zoom view of the first and last pulse. (D) Time profiles. *Key*: *orange*: 450 μmol photons $m^{-2} s^{-1}$; *black*: darkness. The colored bar on top illustrates the light regime with arrows indicating the beginning of a saturation pulse. *Inset*: The average deviation in the sum of concentrations from unity.

oxidases cannot function. Finally, we discuss results obtained from samples illuminated with 590 nm light of 450 μmol photons $m^{-2} s^{-1}$ exposed to ambient oxygen.

3.1.1. Exposure to low light background illumination

After transformation of the singular vectors (Fig. S 2), we obtain the SAS shown in Fig. 2A (SAS_1 and SAS_2 in black and green, respectively). Panel D shows the corresponding concentration profiles of c_1 (black) and c_2 (green) during the entire experiment, while panel B (panel C) zooms into the first (last) saturation pulse. Fig. 2B and C show similar dynamics suggesting that during the second period of darkness the state of the cell is restored and light-induced photodamage can be excluded. As a reminder: one saturation pulse stretches over 1 s with 100 ms time resolution (i.e. ten data points); as light is turned off the signal returns to zero within one data point, meaning that we are unable to resolve relaxation dynamics and the changes in light intensity behave almost like step functions. When the light pulse is turned on at $t = 3$s, however, c_2 *gradually* builds up. This is due to the closure of RCs (consistent with the strong 680 nm signature of SAS_2) which, though very fast, takes one data point (100 ms) to reach a maximum level (F_m). In other words: though not entirely resolved, the so-called OJIP induction phase [36] is, at least, *visible*. Conversely, we interpret c_1 as the population of complexes with open RCs since saturating light results in its sharp decrease (Fig. 2B, C and D). Thus, the interpretation of the two SAS in Fig. 2 can be given in terms of two species depicted in Fig. 1: SAS_2, with the higher amplitude (high fluorescence quantum yield) as PB-PSII complexes with closed RCs (Fig. 1C) and SAS_1, with low quantum yield and little 680 nm signature as PB-PSII complexes with open RCs (Fig. 1A). During saturation pulses, the decrease of c_1 is concomitant with a sharp increase of c_2, whereas during background illumination (F_s), the signal is a combination of both, and consists of fairly constant contributions from complexes with open and closed RCs, with, interestingly, the population of c_1 being the predominant one. The interpretation then is that the background light is able to close only a fraction (ca. 15%, Table 1) of the complexes in the sample as opposed to saturating light. With this background light intensity, the fluorescence dynamics are mainly explained by closing and re-opening of RCs (Fig. 2D) and there is no clear indication of the action of a Hlip-type quencher (vide infra). This pattern systematically reproduces across different experiments with low intensity background light, with cells first dark-adapted for 34, 5 and 1 min (Fig. S 4).

3.1.2. KCN-treated cells exposed to high light background illumination

Fig. 3 shows the results obtained with a sample that was exposed to 450 μmol photons $m^{-2} s^{-1}$ but previously treated with KCN, in order to inhibit terminal oxidase activity. Clearly, the first light pulse (Fig. 3B) induces a rise in c_2, which is by far the predominant species. Correspondingly, SAS_2 (Fig. 3A) has also the higher fluorescence quantum yield and peaks at 681 nm. Therefore, we interpret it as a PB-PSII complex with both RCs closed (Fig. 1C). The interpretation of SAS_1 is less straight forward than in the previous section, because: *i*) the population of c_2 *instantly* reaches a constant level with no sign of an induction phase nor are there correlated increasing/decreasing populations within the first 100 ms; and *ii*) only very small signs of open/closing RCs during saturation pulses are present throughout the experiment (Fig. 3D). Thus, SAS_1 most probably consists of contributions from complexes with quenched species and little complexes with open RCs. As the sample goes through the illumination protocol, c_1 (c_2) gradually increases (decreases) while saturation pulses barely make any difference. Thus, this data matrix is interpretable in terms of the following two species: SAS_2 would correspond to PB-PSII complexes with closed RCs (Fig. 1C) while SAS_1 would correspond to a dynamic mixture of PB-PSII complexes non-photochemically quenched PB-PSII complexes (Fig. 1D) as well as some complexes with open RCs (Fig. 1A). Over time the quenched species become predominant, evidenced by the diminishing signs of open/closing RCs during the saturation pulses

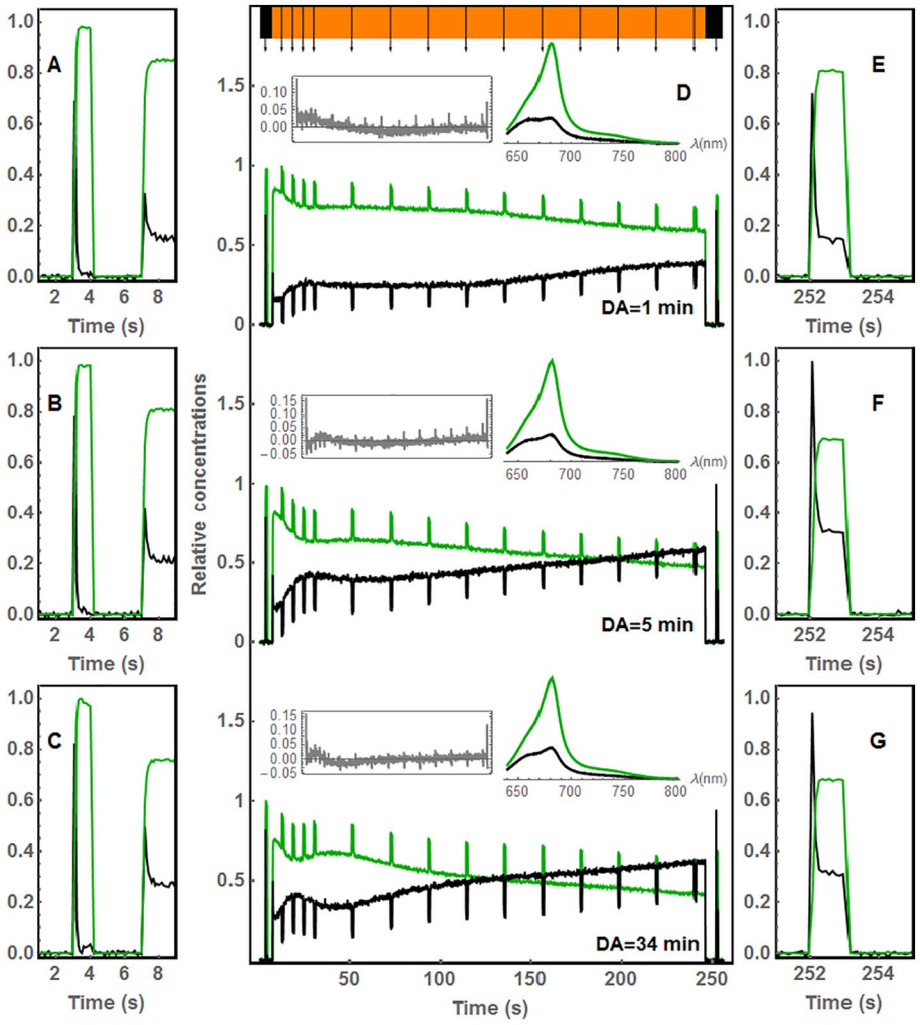

Fig. 6. Three independent analyses of ΔPSI cells with varying dark adaptation. O_2-exposed cells were dark adapted during 1, 5 or 34 min. For each condition, a zoom view of the first (last) pulse is depicted in panels A, B and C (E, F and G). The full light protocol and corresponding SAS (shown as right insets) are depicted on panel D. The colored bar on top illustrates the light regime: 450 μmol photons m^{-2} s^{-1} of 590 nm light (orange) or darkness (black). Left insets depict the average deviation in the sum of concentrations from unity.

(Fig. 3D).

Fig. 4 shows an overlay of the four normalized SASs obtained up to this point: Indeed, the two SAS_2, interpreted in the two experiments as being the same species, are virtually identical. The two SAS_1 are very similar; in the case of the cells not treated with KCN, however, a less pronounced 680 nm signature indicates that energy transfer from the PB terminal emitters to PSII followed by photochemical quenching affects the SAS differently than the quenching of closed complexes by the unknown quencher, Q_X.

3.1.3. Exposure to high-light background illumination in a microoxic environment

In a further attempt to affect respiratory activity without risking an effect on photosynthesis, an experiment was conducted where cells were exposed to 450 μmol photons m^{-2} s^{-1} while a mixture of N_2/CO_2 was bubbled into the cuvette in order to deprive the cells of ambient oxygen. The results are shown in Fig. 5. The obtained SAS and the behavior during the saturation pulses are very similar to the results shown in Fig. 2. As in Fig. 2B and C, the first and last pulses in Fig. 5 clearly show opening/closing behavior and this seems to be a suitable interpretation for the SAS in this case as well. Due to the high background light intensity, however, the F_s levels are now inverted: c_2 is as high as 65% (Table 1) indicating a higher relative concentration of complexes with closed PSII RCs. Otherwise, though there is a modest decrease in c_2 during the first 20 s of background illumination, once the concentration profiles even out, there is no sign of additional fluorescence quenching and most of the signal can be read as constant levels of fluorescence that toggle between distinct levels as a function of the light intensity. This is a remarkable observation, since, under the same background illumination, the KCN experiment reveals the system's ability to quench fluorescence (Fig. 3) and it indicates that oxygen is required for Q_X to function.

3.1.4. Exposure to high light background illumination in an O_2-rich environment

Three experiments with different DA times are shown in Fig. 6. In all cases, cells were exposed to ambient oxygen without addition of KCN. The matrices were analyzed independently, yielding three pairs of concentration profiles shown in Fig. 6D and three pairs of SAS shown as insets therein. Fig. 6A–C and E–G show a zoom in into, respectively, the first and last saturation pulses. These SASs match well those of Fig. 4. Judging from the opening/closing dynamics and the gradual increase of the c_1 base level (concomitant with a decrease in the c_2 base level), the contribution of quenched PB-PSII complexes (Fig. 1D) again gradually increases over time. As previously observed under O_2-deprived conditions (Fig. 5), during the first 20 s of background illumination, c_2 decreases by 15–20% before F_s levels off. However, contrary to those latter conditions, a new phase of fluorescence quenching sets in that lasts until the end of the light protocol. Remarkably, the second quenching phase seems to kick-off at earlier times for samples that underwent a longer DA period. While for the sample with the longest dark adaptation this phase sets in as early as ca. $t = 50$ s, for DA = 5 min it starts around 75 s and for DA = 1 min it only comes at times $t > 140$ s. Also, the relative concentration of c_1 during saturation

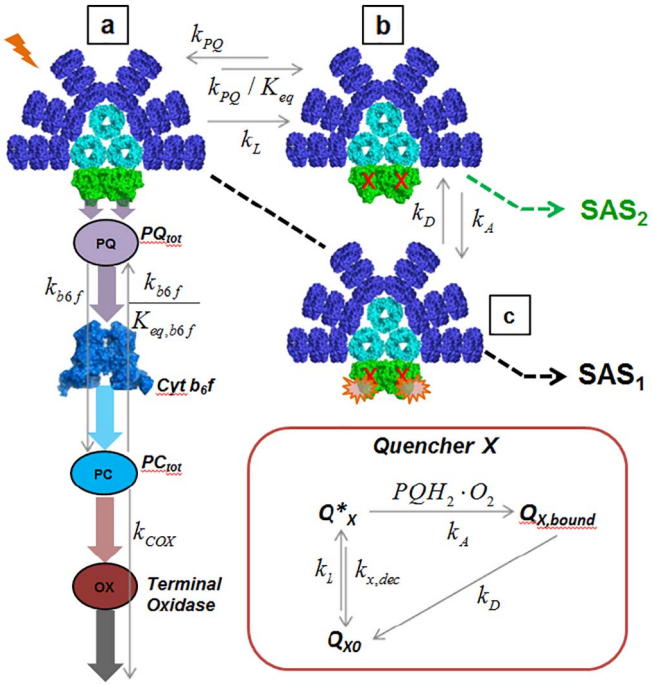

Fig. 7. Scheme summarizing the different species of the mathematical model postulated to describe the time-resolved fluorescence spectra of *Synechocystis* ΔPSI cells. PB-*PSII*-dimers complexes are closed by the action of light or opened via an electron acceptor of the PQ pool (horizontal transition). Additionally, fluorescence quenching can occur if quencher Q_X attaches to a closed RC (vertical transition, detailed in the inset). A PB-PSII complex with two closed RCs (b) emits fluorescence as SAS_2; PB-PSII complexes with either two open RCs (a) or two closed and quenched RCs (c) emit as SAS_1. *Key*: k_L, light-induced transition; k_{PQ}, electron transfer rate to PQ pool; K_{eq}, PQ equilibrium constant, k_A, quencher attachment rate, k_D, quencher detachment rate; $k_{x,dec}$, quencher specific deactivation rate, k_{b6f}, cyt b_6f electron transfer rate; $K_{eq,b6f}$, cyt b_6f equilibrium constant; k_{COX}, terminal oxidase electron transfer rate. Further explanation in the main text and in the SI.

Table 2
Key parameters of the model used to simulate the concentrations of the species depicted in Fig. 7 under different conditions. Common parameters for all conditions are the rates (in s^{-1}) $k_L = 10^{-5}$, $k_{PQ} = 9 \cdot 10^{-3}$, $k_{act} = 0.6$, $k_{x,dec} = 0.02$, $k_A = 3.5 \cdot 10^{-4}$, $k_D = 5 \cdot 10^{-6}$, $k_{b6f} = 0.104$ and the equilibration constants $K_{eq} = 5 \cdot 10^3$ and $K_{eq,b6f} = 5 \cdot 10^{-4}$.

Conditions [Figure]	k_{COX} (s^{-1})	*Rel. conc.* O_2
50 μmol photons m^{-2} s^{-1}		
O_2 + DA = 34 m [8B]	0.01	$4 \cdot 10^{-3}$
450 μmol photons m^{-2} s^{-1}		
O_2 + KCN [9B]	0.001	$4 \cdot 10^{-3}$
ΔO_2 [10B]	0.01	$4 \cdot 10^{-4}$
O_2 + DA = 34 m [11B]	0.01	$4 \cdot 10^{-3}$

pulses tends to reach higher and higher values throughout the experiment. Even after the system has gone through a short relaxation period of a few seconds in darkness, the last saturation pulse does not push the c_1 level down to zero (see Fig. 6E, F and G). Instead, values of around 30% (Table 1), similar to the KCN experiment, are observed in Fig. 6F and G. This again points at a quenched species being formed over time.

3.2. Modeling dark-to-light transitions

3.2.1. Rank 2 systems

To test whether the postulated species described in the sections above could indeed explain the observed dynamics, we constructed a minimal mathematical model (inspired by the model of Ebenhöh et al. [37]) that takes into account only species A, C and D from Fig. 1. We consider PB-PSII-dimer complexes that are fully closed by the action of light or open via an electron acceptor of the PQ pool. Additionally, fluorescence quenching can occur if Q_X attaches to the closed complex. Fig. 7 displays the photosynthetic and respiratory components we consider essential: we postulate three fluorescent components with two distinguishable spectral contributions. Following the interpretation of

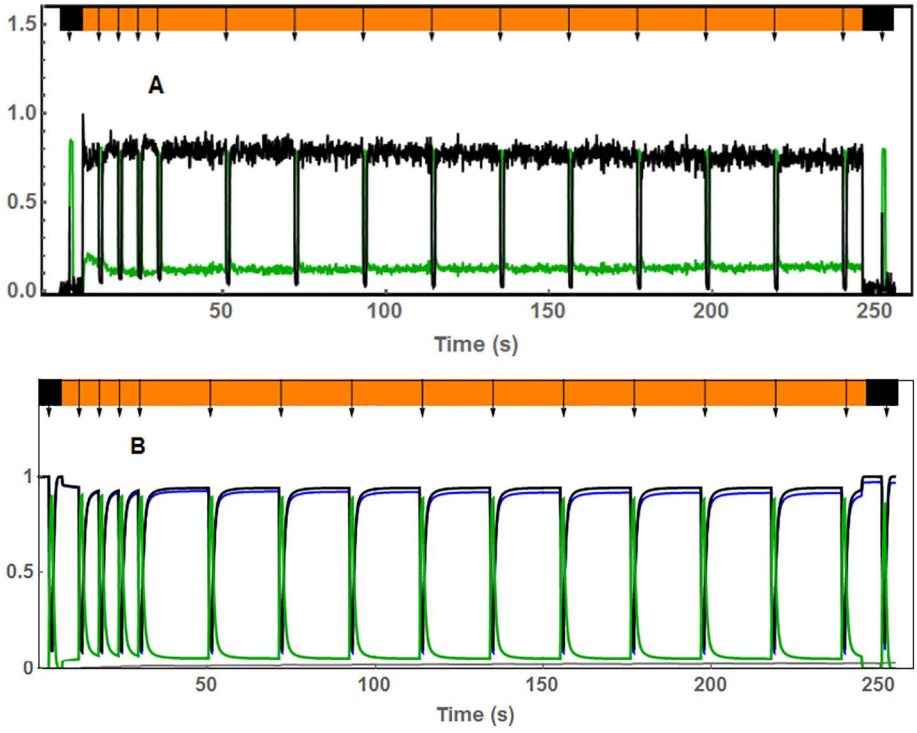

Fig. 8. Spectral decomposition of fluorescence spectra of ΔPSI cells exposed to low background light after 34 min dark adaptation shown in Fig. 2D (A) and simulated concentrations (B) of PB-PSII-dimer complexes with open RCs (blue), with closed RCs and unquenched (green) or quenched (gray). Black represents the sum of blue and gray, and is observed as SAS_1.

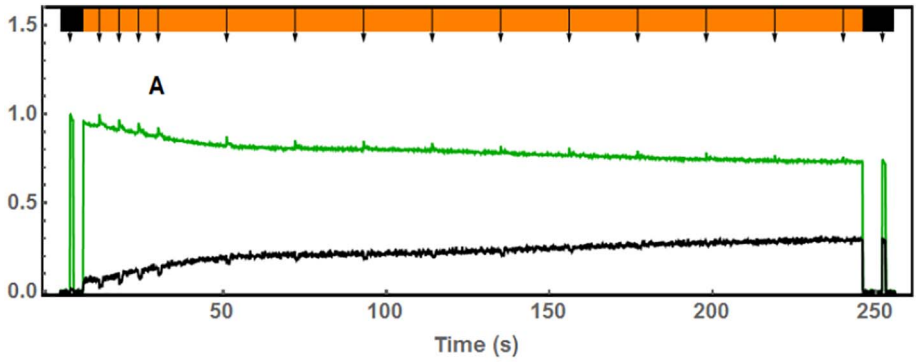

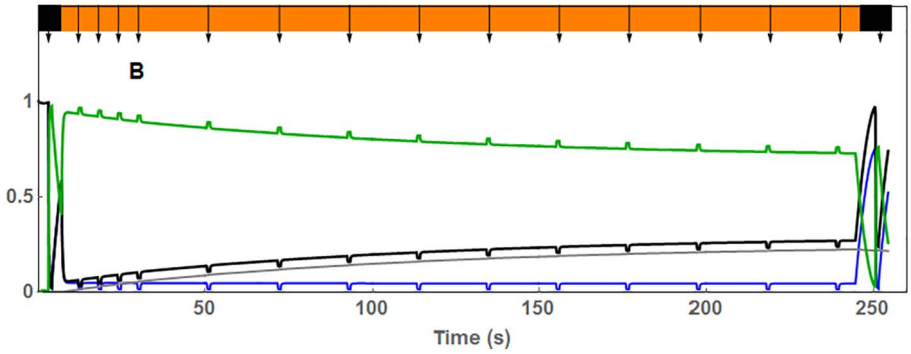

Fig. 9. Spectral decomposition of fluorescence spectra of KCN-treated ΔPSI cells exposed to high background light after 34 min dark adaptation shown in Fig. 3D (A) and simulated concentrations (B) of PB-PSII-dimer complexes with open RCs (blue), with closed RCs and unquenched (green) or quenched (gray). Black represents the sum of blue and gray, and is observed as SAS_1.

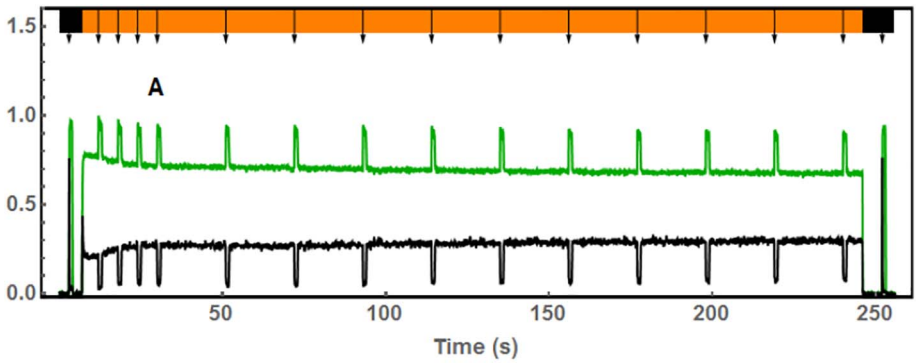

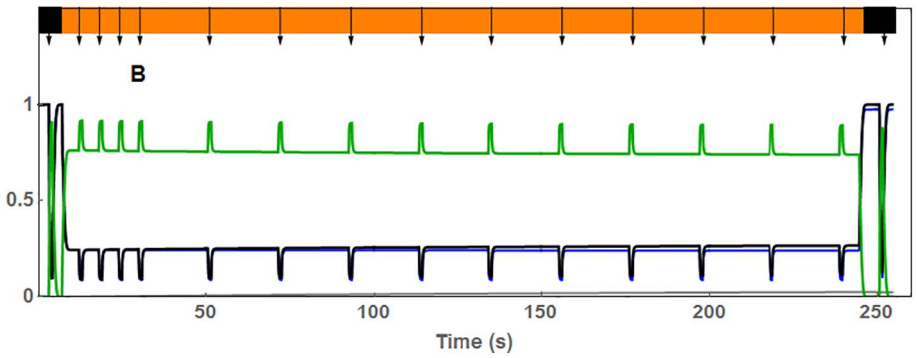

Fig. 10. Spectral decomposition of fluorescence spectra of ΔPSI cells under microoxic conditions exposed to high background light after 34 min dark adaptation shown in Fig. 5D (A) and simulated concentrations (B) of PB-PSII-dimer complexes with open RCs (blue), with closed RCs and unquenched (green) or quenched (gray). Black represents the sum of blue and gray, and is observed as SAS_1.

Fig. 2, there would be two species: a PB-PSII dimer complex with both RCs open as depicted in Fig. 7a, and another one with its RCs closed, as depicted in Fig. 7b. They would emit fluorescence as SAS_1 and SAS_2, respectively. The KCN experiment (Fig. 3D) supports the interpretation of SAS_2 as originating from double-closed RCs, but the quenched component must be attributed to the action of a quencher Q_X. This would result in very similar SAS_1 contributions but two fundamentally different molecular origins. This quenched species is depicted in Fig. 7c and the assumed mechanism for its formation is shown in the red box below: we postulate a light-induced excited state of the quencher Q^*_X that is populated during illumination (k_L) and decays back to its non-activated counterpart, Q_{X0}, with the specific deactivation rate $k_{x,dec}$. Q^*_X is then able to bind to, presumably, PSII. The formation of this $Q_{x,bound}$ is described by an attachment rate k_A and assumed to be proportional to the fraction of reduced PQ, PQH_2, and to the concentration of O_2. In a third step, the quencher detachment rate k_D describes uncoupling of the quencher and a re-population of Q_{X0}. As for the linear electron flow dynamics, the PQ pool is the main electron acceptor of

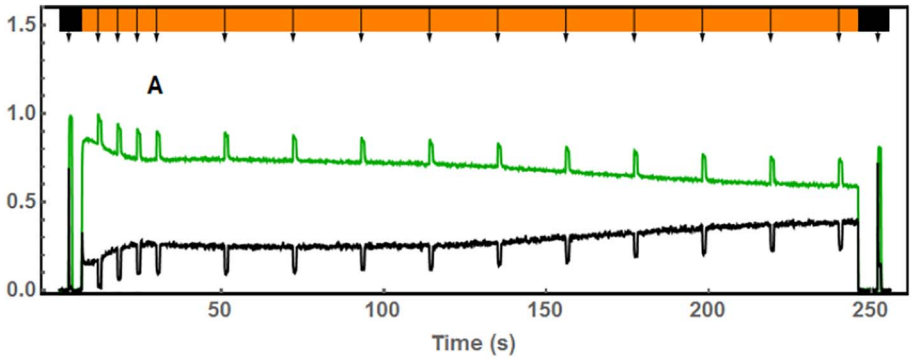

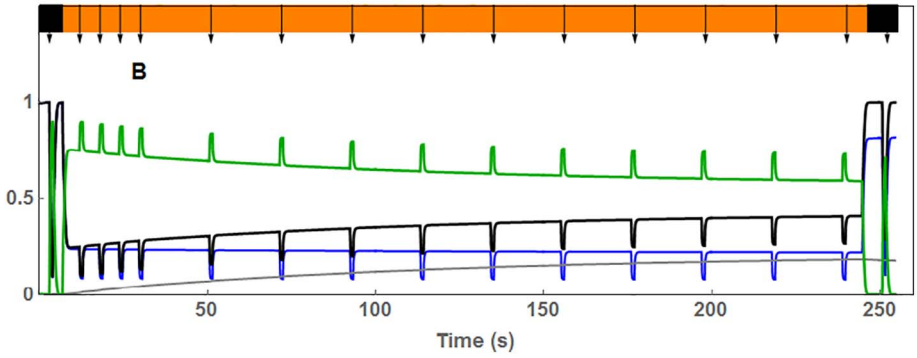

Fig. 11. Spectral decomposition of fluorescence spectra of ΔPSI cells exposed to high background light after 1 min of dark adaptation shown in Fig. 6D, top (A) and simulated concentrations (B) of PB-PSII-dimer complexes with open RCs (blue), with closed RCs and unquenched (green) or quenched (gray). Black represents the sum of blue and gray, and is observed as SAS_1.

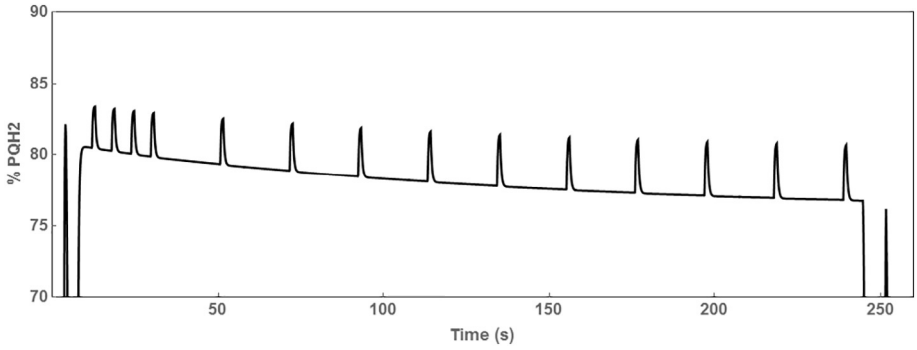

Fig. 12. The redox state of the PQ pool predicted by the model for ΔPSI cells exposed to high background light after 1 min of dark adaptation. The full concentration profile is shown in Fig. S 9.

PSII and works at the rate k_{PQ}. A potential back transfer from the PQ pool to the photosystem is considered in the equilibrium constant K_{eq}. Furthermore, the electrons are carried to the cyt b_6f whose turnover rate is k_{b6f} and which is in equilibrium with the PQ pool with $K_{eq,b6f}$. Finally, the action of the terminal oxidases as acceptors of the PC pool is summed up in the parameter k_{COX} that stands for the last step in the linear electron transport chain. The corresponding system of ordinary differential equations is described in the SI.

Using this model, we set out to simulate results from the analysis presented above. The simulation of the result of the experiment with low background illumination (Fig. 2) is shown in Fig. 8A. A first set of parameters inspired by the model of Matuszyńska et al. [38] was used to simulate the concentration profiles of Fig. 8B. The parameters are collated in Table 2. The general toggle behavior between complexes with open and closed RCs is reproduced fairly well using these values for k_L and k_{PQ}. Moreover, the choice of the equilibrium constants K_{eq} and $K_{eq,b6f}$ and the rates for cyt b_6f and the terminal oxidases k_{b6f} and k_{COX} lead to similar F_m and F_s levels. Note that the simulated concentrations predict the behavior of the species during periods of darkness between the first (last) pulse and the onset (ending) of background illumination, whereas the original data matrix shows a gap because during such dark periods, effectively, no measurement was carried out.

The challenge for the model is to now reproduce the behavior found in the other datasets while tweaking only the parameters that reflect the conditions under which the experiment was carried out. Between the experiments depicted in Figs. 2 and 3, there are two main differences: the background light intensity increases by a factor of 9 and KCN-sensitive electron sinks are chemically blocked. The first parameter, k_L, is adjusted by inputting a different light profile (Fig. S 1), with the right background level. As for the action of KCN on the sample, we decrease the k_{COX} parameter by an order of magnitude: this should reflect, on the one hand, the fact that there is an overall decrease in the turnover rate of terminal oxidases. On the other hand, k_{COX} not being zero, accounts for the assumption that the thylakoid membrane may harbor additional, non-KCN-sensitive electron sinks [39] or that KCN may affect the re-reduction rate of e.g. cyt f [40], ultimately leading to a different, though non-zero, action of the terminal oxidases. Additionally, a mutant which lacks all terminal oxidases has a significantly affected PAM profile [41], compatible with that of KCN-treated cells presented in this work. Small changes in the parameters k_{COX} and k_L already lead to Fig. 9B (changed parameters are written in bold in Table 2). A higher background light intensity leads to an overall increase of the c_2 level. Additionally, a considerable drop in k_{COX} translates in the inability to drain electrons from the PC pool which, then again, leads to complete reduction of the PQ pool and a further increase in the F_s level, almost to the point that saturation pulses barely stand out (almost no variable fluorescence

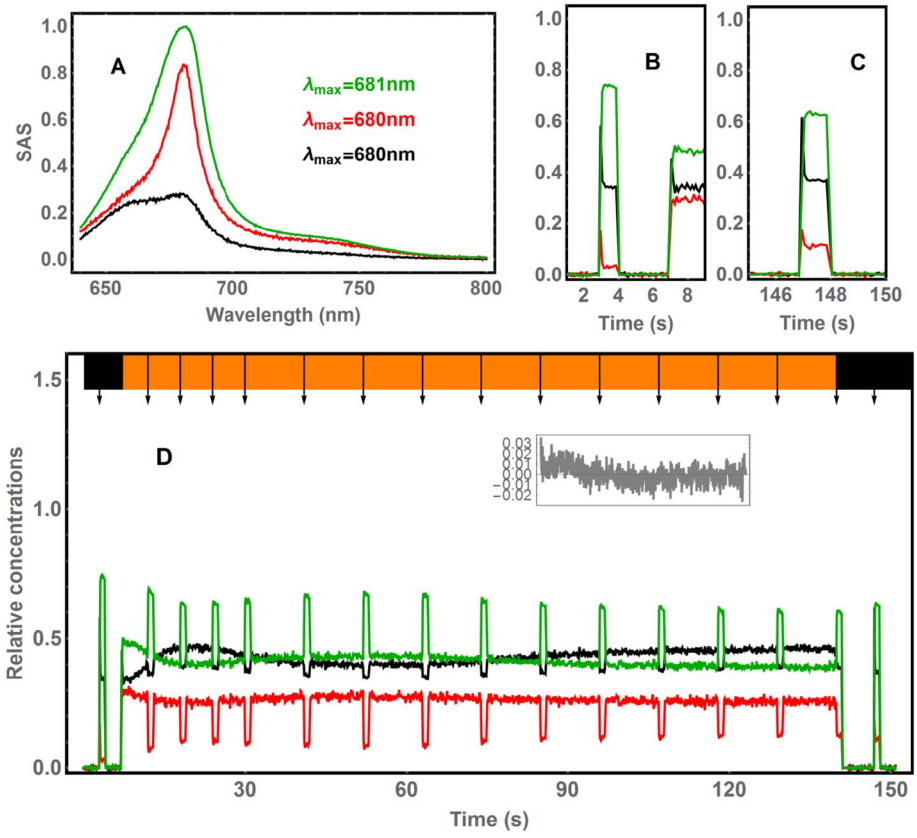

Fig. 13. Spectral decomposition of fluorescence spectra of ΔPSI cells exposed to high background light and ambient O_2 after 1 min of dark-adaptation. (A) The SAS (black: SAS_1; green: SAS_2 red: SAS_3) obtained after transformation of the singular vectors (shown in Fig. S 7). Panels B and C show a zoom view of the first and last pulse. (D) Time profiles. *Key*: *orange*: 450 μmol photons m^{-2} s^{-1}; *black*: darkness. The colored bar on top illustrates the light regime (Fig. S 1C) with arrows indicating the beginning of a saturation pulse. *Inset*: Average deviation in the sum of concentrations from unity.

detectable). If the signal decreases over time, it is because of the action of a quencher Q_X that forms quenched complexes over time (solid gray curve) and is observed as the black SAS_1. The deactivation of Q_X happens slowly enough that after turning the background light off, the gray level lingers on. The remaining Q_X explains why the black level in the last pulse of the KCN-treated sample (Fig. 3C) decreases to 30% instead of zero.

As a next step, we now restore the k_{COX} parameter to its original value and decrease, instead, the concentration of O_2 by one order of magnitude. The result is shown in Fig. 10: restoring k_{COX} is a sensible choice given the magnitude of the observed variable fluorescence. Concomitantly, the absence of O_2 directly impacts the quencher kinetics (cf. the SI). Since nearly no quencher is formed, the overall levels of both c_1 and c_2 remain fairly constant throughout the experiment, as indeed observed. This would reinforce the hypothesis that Q_X is operative in the presence of oxygen in order to hamper the formation of singlet oxygen or any other ROS.

In principle, restoring the oxygen value to its original value should then describe the experiment series shown in Fig. 6. This is illustrated in Fig. 11. The first striking observation is that, although variable fluorescence and an overall decrease of the F_s level in c_2 are reproduced to some extent, the data shows particular moments in time where fluorescence quenching sets in. The first decrease in c_2 happens within the first 20–40 s of background illumination and it is visible in all samples. Depending on the length of the DA, a second phase sets in with c_2 steadily decreasing until the end of the light protocol. There are two clear exceptions: *i*) in the case of low background light and *ii*) in the microoxic environment, the second phase does not set in.

The current model, however, does not yet explain how dark-adaptation relates to the specific evolution of the fluorescence spectrum over time. Nevertheless, the model does offer a prediction concerning the behavior of the redox potential throughout the experiment: the redox state of the PQ pool (generally considered as a key regulator in cyanobacteria; see *e.g.* [9]) follows the trend of the SAS_2 concentration and is predicted to be much higher (Fig. 12) than reported for the wild type under high light [42]. This is in line with the high degree of reduction of the PQ pool observed in this mutant by indirect measurements in similar light conditions [5]. It is not known whether the biochemical mechanism(s) of state transitions are still operative in the PSI-deletion strain. The ease of modulation of the redox state of the PQ pool might suggest they are; the actual regulatory parameter, however, may be the redox state of the cyt b_6f complex [42].

3.2.2. *Beyond the rank 2 analysis*

Further limitations to the model arise with data matrices of higher rank. Fig. 13 shows a dataset where the fluorescence signal was acquired with another light protocol where the sampling frequency of the saturation pulses was increased (Fig. S 1C) and with another batch of ΔPSI cells. The response is highly dynamic and visual inspection of the singular value scree plot (Fig. S 7) already points out that, at least, a third component is clearly distinguishable from the noise. Here too, the black and green are interpreted as a PB-PSII dimer complex with closed and open RCs, respectively (compare with SASs in Fig. 6A), and display during the first 50 s a mutual exchange in populations with the third component (red) nearly being constant (Fig. 6D). The third component could be an intermediate state such as the one depicted in Fig. 1B where one RC in the PSII dimer is closed but not the other. An alternative may include a PB-PSII complex with closed RCs but able to alleviate the excitation pressure by transferring energy to e.g. Flv2/4 [43], resulting in less back-transfer to PB which manifests as a less pronounced 660 nm emission than that of SAS_2. Additional measurements of expression levels of the Flv2/4 proteins would have to support this hypothesis, but regardless of the mechanism, none of these two interpretations would contradict the behavior of the (red) time profile c_3, which decreases during the pulses, contributing thus to the population of c_2 (which systematically has maximal values during saturation periods). This alternating pattern in the concentration of certain complexes illustrates the dynamic character of the response to light exposure. It is unclear

which and how many molecular origins such a re-arrangement of complexes might be resulting from. Recently, however, small-angle neutron scattering experiments in *Synechocystis* cells have revealed a substantial re-configuration of the interthylakoidal space in the event of a dark-to-light transition [44,45]. Also, in the case of the PAL mutant lacking phycobilisomes, a rapid (2–4 min) re-organization of the thylakoidal surface is observed which the authors suggest could originate from surface charges [44]. These interpretations, as well as the speculation that the contribution of the fourth singular value (Fig. S 7) may be non-negligible present a scenario, however, that goes beyond the scope of the minimal model presented in this work.

4. Closing remarks

In the series of experiments that were all analyzed as independent rank 2 systems, the two SASs are interpreted as follows: SAS_2: PB-PSII complexes with closed RCs and SAS_1 as the same complex being quenched either photochemically or non-photochemically by an Hlip-type quencher as illustrated in Fig. 7. Addition of KCN leads to almost vanishing variable fluorescence and this decrease is attributed to the formation of a quenched complex that, as Fig. 10 suggests, requires the presence of O_2. The time behavior of the quenched component in samples without DCMU is correlated with DA time. The longer the cell performs respiratory activity in darkness the earlier does the quencher respond to background illumination. This work comes to show that *Synechocystis* possesses an impressive degree of plasticity when it comes to generating functional sinks for excitations in the absence of PSI. The mechanisms revealed in this work could inspire future efforts attempting to model more complex systems such as the wild-type organism.

Transparency document

The Transparency document associated with this article can be found, in the online version.

Acknowledgements

Joris Snellenburg is thanked for helpful discussions. AMA gratefully acknowledges Michael Reus for his valuable assistance in re-building the multiple LED set-up in Amsterdam. Roberta Croce and Alfred Holzwarth are thanked for letting us use this set-up. The ΔPSI mutant which was originally constructed by Wim Vermaas (Arizona State University, Tempe, Arizona, U.S.) was kindly provided to us by Prof. Christiane Funk (Umeå University, Sweden). This research was performed as part of the BioSolar Cells research programme, sponsored by the Dutch Ministry of Economic Affairs. This work is part of the research program of the Netherlands Organization for Scientific Research (NWO, previously FOM).

Appendix A. Supplementary data

Supplementary data to this article can be found online at https://doi.org/10.1016/j.bbabio.2017.11.002.

References

[1] L.-N. Liu, Distribution and dynamics of electron transport complexes in cyanobacterial thylakoid membranes, Biochim. Biophys. Acta 1857 (2015) 256–265.
[2] S. Scherer, H. Almon, P. Böger, Interaction of photosynthesis, respiration and nitrogen fixation in cyanobacteria, Photosynth. Res. 15 (1988) 95–114.
[3] C.W. Mullineaux, Electron transport and light-harvesting switches in cyanobacteria, Front. Plant Sci. 5 (2014) 7.
[4] T. Ogawa, K. Sonoike, Dissection of respiration and photosynthesis in the cyanobacterium *Synechocystis* sp. PCC6803 by the analysis of chlorophyll fluorescence, J. Photochem. Photobiol. B Biol. 144 (2015) 61–67.
[5] J.W. Cooley, W.F.J. Vermaas, Succinate dehydrogenase and other respiratory pathways in thylakoid membranes of *Synechocystis* sp. strain PCC 6803: capacity comparisons and physiological function, J. Bacteriol. 183 (2001) 4251–4258.
[6] R.M. Schuurmans, J.M. Schuurmans, M. Bekker, J.C. Kromkamp, H.C.P. Matthijs, K.J. Hellingwerf, The redox potential of the plastoquinone pool of the cyanobacterium *Synechocystis* species strain PCC 6803 is under strict homeostatic control, Plant Physiol. 165 (2014) 463–475.
[7] D. Shevela Govindjee, Adventures with cyanobacteria: a personal perspective, Front. Plant Sci. 2 (2011) 28.
[8] D.J. Lea-Smith, P. Bombelli, R. Vasudevan, C.J. Howe, Photosynthetic, respiratory and extracellular electron transport pathways in cyanobacteria, Biochim. Biophys. Acta Bioenerg. 1857 (2016) 247–255.
[9] L.-N. Liu, S.J. Bryan, F. Huang, J. Yu, P.J. Nixon, P.R. Rich, C.W. Mullineaux, Control of electron transport routes through redox-regulated redistribution of respiratory complexes, Proc. Natl. Acad. Sci. 109 (2012) 11431–11436.
[10] V. Chukhutsina, L. Bersanini, E.-M. Aro, H. van Amerongen, Cyanobacterial flv4-2 operon-encoded proteins optimize light harvesting and charge separation in photosystem II, Mol. Plant 8 (2015) 747–761.
[11] H. Mi, T. Endo, U. Schreiber, T. Ogawa, K. Asada, Electron donation from cyclic and respiratory flows to the photosynthetic intersystem chain is mediated by pyridine nucleotide dehydrogenase in the cyanobacterium *Synechocystis* PCC 6803, Plant Cell Physiol. 33 (1992) 1233–1237.
[12] Y. Helman, D. Tchernov, L. Reinhold, M. Shibata, T. Ogawa, R. Schwarz, I. Ohad, A. Kaplan, Genes encoding A-type flavoproteins are essential for photoreduction of O_2 in cyanobacteria, Curr. Biol. 13 (2003) 230–235.
[13] J.B. Vicente, C.M. Gomes, A. Wasserfallen, M. Teixeira, Module fusion in an A-type flavoprotein from the cyanobacterium *Synechocystis* condenses a multiple-component pathway in a single polypeptide chain, Biochem. Biophys. Res. Commun. 294 (2002) 82–87.
[14] M.J. Behrenfeld, K.H. Halsey, A.J. Milligan, Evolved physiological responses of phytoplankton to their integrated growth environment, Philos. Trans. R. Soc., B 363 (2008) 2687–2703.
[15] D. Kirilovsky, R. Kaňa, O. Prášil, Mechanisms modulating energy arriving at reaction centers in cyanobacteria, in: B. Demmig-Adams, G. Garab, W. Adams, IIIGovindjee (Eds.), Non-photochemical Quenching and Energy Dissipation in Plants, Algae and Cyanobacteria, Springer, Dordrecht, 2014, pp. 471–502.
[16] A. Wilson, C. Punginelli, A. Gall, C. Bonetti, M. Alexandre, J.-M. Routaboul, C.A. Kerfeld, R. van Grondelle, B. Robert, J.T.M. Kennis, D. Kirilovsky, A photoactive carotenoid protein acting as light intensity sensor, Proc. Natl. Acad. Sci. U. S. A. 105 (2008) 12075–12080.
[17] M. Gwizdala, A. Wilson, D. Kirilovsky, In vitro reconstitution of the cyanobacterial photoprotective mechanism mediated by the orange carotenoid protein in *Synechocystis* PCC 6803, Plant Cell 23 (2011) 2631–2643.
[18] L. Tian, I.H.M. van Stokkum, R.B.M. Koehorst, A. Jongerius, D. Kirilovsky, H. van Amerongen, Site, rate, and mechanism of photoprotective quenching in cyanobacteria, J. Am. Chem. Soc. 133 (2011) 18304–18311.
[19] C.W. Mullineaux, J.F. Allen, State 1-state 2 transitions in the cyanobacterium *Synechococcus* 6301 are controlled by the redox state of electron carriers between photosystems I and II, Photosynth. Res. 23 (1990) 297–311.
[20] D. Kirilovsky, Modulating energy arriving at photochemical reaction centers: orange carotenoid protein-related photoprotection and state transitions, Photosynth. Res. 126 (2015) 3–17.
[21] C.W. Mullineaux, D. Emlyn-Jones, State transitions: an example of acclimation to low-light stress, J. Exp. Bot. 56 (2005) 389–393.
[22] A.M. Acuña, R. Kaňa, M. Gwizdala, J.J. Snellenburg, P. van Alphen, B. van Oort, D. Kirilovsky, R. van Grondelle, I.H.M. van Stokkum, A method to decompose spectral changes in *Synechocystis* PCC 6803 during light-induced state transitions, Photosynth. Res. 130 (2016) 237–249.
[23] W.F.J. Vermaas, G. Shen, S. Styling, Electrons generated by photosystem II are utilized by an oxidase in the absence of photosystem I in the cyanobacterium *Synechocystis* sp. PCC 6803, FEBS Lett. 337 (1994) 103–108.
[24] M. Havaux, G. Guedeney, Q. He, A.R. Grossman, Elimination of high-light-inducible polypeptides related to eukaryotic chlorophyll a/b-binding proteins results in aberrant photoacclimation in *Synechocystis* PCC6803, Biochim. Biophys. Acta Bioenerg. 1557 (2003) 21–33.
[25] H. Staleva, J. Komenda, M.K. Shukla, V. Šlouf, R. Kaňa, T. Polívka, R. Sobotka, Mechanism of photoprotection in the cyanobacterial ancestor of plant antenna proteins, Nat. Chem. Biol. 11 (2015) 287–291.
[26] J. Komenda, R. Sobotka, Cyanobacterial high-light-inducible proteins — protectors of chlorophyll–protein synthesis and assembly, Biochim. Biophys. Acta Bioenerg. 1857 (2016) 288–295.
[27] R.K. Sinha, J. Komenda, J. Knoppová, M. Sedlářová, P. Pospíšil, Small CAB-like proteins prevent formation of singlet oxygen in the damaged photosystem II complex of the cyanobacterium *Synechocystis* sp. PCC 6803, Plant Cell Environ. 35 (2012) 806–818.
[28] J.W. Chidgey, M. Linhartova, J. Komenda, P.J. Jackson, M.J. Dickman, D.P. Canniffe, P. Konik, J. Pilny, C.N. Hunter, R. Sobotka, A cyanobacterial chlorophyll synthase-HliD complex associates with the Ycf39 protein and the YidC/Alb3 insertase, Plant Cell 26 (2014) 1267–1279.
[29] R. Kaňa, O. Prášil, O. Komárek, G.C. Papageorgiou, Govindjee, Spectral characteristic of fluorescence induction in a model cyanobacterium, *Synechococcus* sp. (PCC 7942), Biochim. Biophys. Acta 1787 (2009) 1170–1178.
[30] R. Kaňa, E. Kotabová, O. Komárek, B. Šedivá, G.C. Papageorgiou, Govindjee, O. Prášil, The slow S to M fluorescence rise in cyanobacteria is due to a state 2 to state 1 transition, Biochim. Biophys. Acta 1817 (2012) 1237–1247.
[31] G. Shen, S. Boussiba, W.F.J. Vermaas, *Synechocystis* sp. PCC 6803 strains lacking photosystem I and phycobilisome function, Plant Cell 5 (1993) 1853–1863.
[32] P.H. Lambrev, M. Nilkens, Y. Miloslavina, P. Jahns, A.R. Holzwarth, Kinetic and

spectral resolution of multiple nonphotochemical quenching components in Arabidopsis leaves, Plant Physiol. 152 (2010) 1611–1624.
[33] M.A. Orman, M.P. Brynildsen, Inhibition of stationary phase respiration impairs persister formation in *E. coli*, Nat. Commun. 6 (2015) 7983.
[34] D. Pils, G. Schmetterer, Characterization of three bioenergetically active respiratory terminal oxidases in the cyanobacterium *Synechocystis* sp. strain PCC 6803, FEMS Microbiol. Lett. 203 (2001) 217–222.
[35] G. Golub, C. Van Loan, The singular value decomposition and unitary matrices, Matrix Computations, 1996, pp. 70–71.
[36] A. Stirbet, Govindjee, On the relation between the Kautsky effect (chlorophyll a fluorescence induction) and photosystem II: basics and applications of the OJIP fluorescence transient, J. Photochem. Photobiol. B Biol. 104 (2011) 236–257.
[37] O. Ebenhöh, G. Fucile, G. Finazzi, J.-D. Rochaix, M. Goldschmidt-Clermont, Short-term acclimation of the photosynthetic electron transfer chain to changing light: a mathematical model, Philos. Trans. R. Soc., B 369 (2014) 20130223.
[38] A. Matuszyńska, S. Heidari, P. Jahns, O. Ebenhöh, A mathematical model of non-photochemical quenching to study short-term light memory in plants, Biochim. Biophys. Acta Bioenerg. 1857 (2016) 1860–1869.
[39] Y. Allahverdiyeva, H. Mustila, M. Ermakova, L. Bersanini, P. Richaud, G. Ajlani, N. Battchikova, L. Cournac, E.-M. Aro, Flavodiiron proteins Flv1 and Flv3 enable cyanobacterial growth and photosynthesis under fluctuating light, Proc. Natl. Acad. Sci. 110 (2013) 4111–4116.
[40] C. Büchel, O. Zsíros, G. Garab, Alternative cyanide-sensitive oxidase interacting with photosynthesis in *Synechocystis* PCC6803. Ancestor of the terminal oxidase of chlororespiration? Photosynthetica 35 (1998) 223–231.
[41] R.M. Schuurmans, P. van Alphen, J.M. Schuurmans, H.C. Matthijs, K.J. Hellingwerf, Comparison of the photosynthetic yield of cyanobacteria and green algae: different methods give different answers, PLoS One 10 (2015) e0139061.
[42] R.M. Schuurmans, J.C.P. Matthijs, K.J. Hellingwerf, Transition from exponential to linear photoautotrophic growth changes the physiology of *Synechocystis* sp. PCC 6803, Photosynth. Res. 132 (2017) 69–82.
[43] P. Zhang, Y. Allahverdiyeva, M. Eisenhut, E.-M. Aro, Flavodiiron proteins in oxygenic photosynthetic organisms: photoprotection of photosystem II by Flv2 and Flv4 in *Synechocystis* sp. PCC 6803, PLoS One 4 (2009) e5331.
[44] G. Nagy, D. Posselt, L. Kovács, J.K. Holm, M. Szabó, B. Ughy, L. Rosta, J. Peters, P. Timmins, G. Garab, Reversible membrane reorganizations during photosynthesis in vivo: revealed by small-angle neutron scattering, Biochem. J. 436 (2011) 225–230.
[45] M. Liberton, L.E. Page, W.B. O'Dell, H. O'Neill, E. Mamontov, V.S. Urban, H.B. Pakrasi, Organization and flexibility of cyanobacterial thylakoid membranes examined by neutron scattering, J. Biol. Chem. 288 (2013) 3632–3640.